Desalination and Water Treatment
www.deswater.com

doi: 10.5004/dwt.2022.28889

273 (2022) 190–202
October

Disparate soil textures as a native medium for As(V) and Pb(II) separation from aqueous systems

Tijana Stanišić[a,*], Maja Đolić[b], Mirjana Ćujić[c], Mirjana Ristić[b], Aleksandra Perić Grujić[b]

[a]*Innovation Center of the Faculty of Technology and Metallurgy, 4 Karnegijeva Street, Belgrade, Serbia, email: tstanisic@tmf.bg.ac.rs*
[b]*University of Belgrade, Faculty of Technology and Metallurgy, 4 Karnegijeva Street, Belgrade, Serbia, emails: mdjolic@tmf.bg.ac.rs (M. Đolić), risticm@tmf.bg.ac.rs (M. Ristić), alexp@tmf.bg.ac.rs (A. Perić Grujić)*
[c]*University of Belgrade, Vinča Institute of Nuclear Sciences – National Institute of the Republic of Serbia, 12–14 Mike Petrovića Alasa Street, Vinča, Belgrade, Serbia, email: cujicm@vin.bg.ac.rs*

Received 27 April 2022; Accepted 17 August 2022

ABSTRACT

This study investigated the use of different natural raw soil materials as low-cost adsorbents for the removal to remove As(V) and Pb(II) from aqueous systems. It deals with the effect of different soil textures, sandy loam, loam, and loamy sand, on adsorption efficiency. Fourier-transform infrared spectroscopy (FTIR) was used to carry out the comprehensive characterization of materials, as well as scanning electron microscopy (SEM), X-ray diffraction (XRD), and liquid nitrogen porosimetry or the Brunauer–Emmett–Teller (BET). Studies were performed in a batch system; the initial concentration of examined heavy metals was 100 $\mu g \cdot L^{-1}$, pH varied in the range of 4–6, and the adsorbent dosage was 5–20 mg/10 mL. Sandy loam was the most efficient adsorbent for As(V) separation, with a maximum removal efficiency of 47.5%, while the loam was the most efficient for Pb(II) separation, with a maximum removal efficiency of 94.2%. The removal efficiency was affected mainly by the adsorbent characteristics. Performed kinetic studies revealed two steps of adsorption for both investigated ions. Obtained results indicate that natural sorbents used in this work present environmentally sustainable material for As(V) and Pb(II) removal, on the one hand, and the basis for further studies on the simultaneous removal of heavy metals from water and their reduced mobility in soil, on the other.

Keywords: Natural adsorbents; Heavy metals; Material characterization; Batch studies; Chemical kinetics

1. Introduction

Heavy metals are widely spread throughout the environment, and their presence can cause environmental problems and negative consequences for human health [1]. Usually, they reach water courses by uncontrolled discharge of various industrial wastewaters into water intakes and *via* industrial chemicals such as fertilizers, pesticides, herbicides, paints, varnishes, pigments, etc. [2,3]. Lead is an industrial pollutant of particular interest because of its toxicity and widespread presence in the environment [3,4]. It is widely utilized in many industries such as transportation, agriculture, mining, ceramic, metal plating, paints, and battery production [5,6]. This heavy metal enters the human body through contaminated water, food, and air, causing anemia, kidney disease, tissue damage to the brain, and even death in extreme poisoning situations [7,8]. Arsenic is a ubiquitous element that occurs in water due to various natural (mineral dissolution and natural soil drainage) and anthropogenic (mining exploitation, agricultural pesticides,

* Corresponding author.

disposal of fly ash) activities [9]. Metal(loid)s such as arsenic also have adverse effects on human health, with long-term exposure to arsenic being linked to skin, lung, bladder, kidney, and liver cancers and other non-cancerous diseases such as diabetes, blood pressure, and reproductive disorders [10]. Due to their toxicity, the permission concentration of lead and arsenic in drinking water, according to the United State Environmental Protection Agency (USEPA) and the World Health Organization (WHO), is set to 15 and 10 $\mu g \cdot L^{-1}$ for Pb(II) ion, respectively, and 10 $\mu g \cdot L^{-1}$ for As(V) ion [11,12].

Removing heavy metals from surface water, wastewater, and water for human consumption (drinking and recreation) is a major problem and challenge today. Several developed techniques are used to remove heavy metals from aqueous solutions, and the most common ones are chemical precipitation, electrochemical treatment, ion exchange, filtration, membrane processes, and adsorption [13]. Although each technique has its advantages and disadvantages, more and more research is focused on the development and application of efficient and cost-effective technologies for water purification. Due to its low cost, availability, and flexibility, adsorption is a process that has been widely used to remove heavy metals from the aquatic ecosystem [14].

In addition, a wide range of materials can be used as a separation medium for heavy metal removal from aqueous solutions. Nowadays, scientific research examines new materials, and the use of alternative, widely available, natural, and cheap materials such as zeolite, clay, minerals, biosorbents, and many others [15,16]. Natural materials can be considered sustainable nature-based adsorbents due to their abundance and availability. Those materials need good mechanical properties, such as strength and resistance to destruction, high internal surface area, appropriate size distribution, chemical properties, and type of functional groups present, to be applied as adsorbents [17]. The adsorption of lead and arsenic is mainly governed by various physicochemical characteristics of soil such as pH, soil texture, cation exchange capacity, organic matter, oxides and hydroxides, the presence of microorganisms, occurrence and form of anions/cations, the content of macro and micronutrients, oxidation-reduction potential, sorption capacity and resistance of the soil [18,19]. Soil ingredients usually have lower adsorption capacity for the removal of As(V), but the presence of Iron (Fe) and Manganese (Mn) in the form of their oxides, hydroxides, and oxyhydroxides in the soil improves the binding affinity of As(V) [20].

In this work, the native form of soil with different textures (sandy loam, loam, and loamy sand) was applied for the separation of Pb(II) and As(V) from the aqueous system. Lead and arsenic, pollutants with profound health impact, were selected for this research, to follow the influence of analyte ionic form, since in aqueous solution, lead is in cationic, and arsenic in anionic form. Additionally, research was directed to elucidate possible adsorption mechanisms, including the optimal reaction conditions.

2. Materials and methods

The soil samples were collected from Northern Portugal. Before analysis, soil samples were mesh-sieved (2 mm), washed with Milli-Q water (18.2 MΩ cm), dried for 120 min at 105°C, and stored in desiccators before further experimental procedures. Dried samples were homogenized using a pestle and a mortar without chemical activation.

2.1. Material characterization

The samples mineralogy was characterized using the X-ray diffraction method – XRD (type of instrument: ENRAF NONIUS FR590 XRD, Bruker AXS, MA, USA), diffractometer at Cu Kα 1.2 radiation and a step size of 0.05° and a step time of 1 s. After that, the FA/FAG's XRD pattern was analyzed in relation to the diffraction powder file (PDF2) for the following components:

- Sample A: Quartz, α-SiO_2 (reference pattern: 85-0794), Microcline maximum, $KAlSi_3O_8$ (76-0918), Potassium iron silicate, $K_{1.11}(Fe_{1.11}Si_{0.89}O_4)$ (81-2005), Cristobalite beta (high), SiO_2 (89-3607) and Kaolinite, $Al_2(Si_2O_5)(OH)_4$ (89-6538);
- Sample B: Quartz, α-SiO_2 (reference pattern: 85-0794), Kaolinite, $Al_2(Si_2O_5)(OH)_4$ (89-6538), Cristobalite beta (high), SiO_2 (89-3607), and Microcline maximum $KAlSi_3O_8$ (76-0918);
- Sample C: Quartz, α-SiO_2 (reference pattern: 85-0794), Kaolinite, $Al_2(Si_2O_5)(OH)_4$ (89-6538), Cristobalite beta (high), SiO_2 (89-3607), and Potassium Iron Silicate, $K_{1.11}(Fe_{1.11}Si_{0.89}O_4)$ (81-2005).

Surface functional groups of samples were determined using the Fourier-transform infrared spectroscopy – FTIR, within the range of 400–4,000 cm^{-1}, at 4 cm^{-1} of spectral resolution (type of instrument: BOMEM spectrometer, Hartmann & Brown). Samples were made as KBr pellets at 22°C, and measurements were conducted in the range of 500–4,000 cm^{-1}. The physicochemical structure of the surface morphology was examined by scanning electron microscopy – SEM (type of instrument: TESCAN MIRA 3 XMU). The textural properties of tested samples were analyzed using liquid nitrogen porosimetry or the Brunauer–Emmett–Teller – BET adsorption-desorption isotherms, measured by Micrometrics ASAP 2020 V 1.05 H surface area analyzer.

2.2. Batch adsorption experiments

The adsorption of As(V) and Pb(II) ions was conducted in a batch system, with initial concentrations of 100 $\mu g \cdot L^{-1}$ for both elements. In order to determine the optimal experimental conditions, the mass of the adsorbent (5–20 mg) and solution pH 4, 5, and 6 were varied, while agitation time (24 h) and temperature (25°C) were kept constant. Solutions of 0.1 M NaOH and 0.1 M HNO_3 were used for pH adjustment. Shaking the adsorbents in 10 mL of solution for 24 h was performed using a laboratory shaker (200 rpm). After the adsorption process, the samples were filtered through a 0.45-μm pore diameter membrane filter and acidified with nitric acid (1:1, v/v) before examining ions' analytical determination.

The concentration of As(V) and Pb(II) was determined using inductively coupled plasma mass spectrometry

(ICP-MS) on an Agilent 7500ce ICP-MS system (Waldbronn, Germany) equipped with an octopole collision/reaction cell, the Agilent 7500ce ICP-MS ChemStation software, a MicroMist nebulizer, and a Peltier cooled (2_C) quartz Scott-type double pass spray chamber. Calibration of ICP-MS was performed using external standards. The method validation was performed based on certified reference material – SLRS (River Water Reference Material for Trace Metals, National Research Council Canada, Ottawa, Ontario, Canada).

The adsorption capacity of the adsorbent (q) and the removal percentage (% R) were calculated according to the following equations:

$$q = \frac{c_i - c_e}{m} \times V \tag{1}$$

$$\%R = \left(\frac{c_i - c_e}{c_i} \right) \times 100 \tag{2}$$

where c_i and c_e are the concentrations of examined ion in the solution (μg·L^{-1}) at the beginning and in the equilibrium, respectively. V is the volume of solution (mL), and m is the adsorbent dosage (mg).

2.3. Kinetic study

The kinetic study was performed to evaluate sorption rates and adsorption mechanisms of Pb(II) and As(V) onto the natural materials. The batch adsorption experiments were performed for constant Pb(II) and As(V) initial concentration (100 μg·L^{-1}), adsorbent dosage (10 mg), and specific intervals (5, 30, 60, 90, 360, and 1,440 min).

The kinetics of the adsorption process was analyzed by a nonlinear (3a–6a) and linear (3b–6b) least-squares method in the form of pseudo-first (PFO), pseudo-second (PSO) order, and intraparticle diffusion model. The kinetic models used for data fitting are presented in Table 1.

3. Results and discussion

3.1. Material characterization

The samples are categorized as A – sandy loam (69.6% sand, 26.0% silt, 4.4% clay), B – loam (43.5% sand, 34.8% silt, 21.7% clay), and C – loamy sand (82% sand, 12% silt, 6% clay) (Table 2), according to the USDA soil texture triangle, developed by the U.S. Department of Agriculture (USDA) (Fig. 1). Each soil texture is characterized by specific particle size, bulk density, water retention capacity, and permeability.

3.1.1. XRD analysis

The XRD structural analyses of sandy loam (A), loam (B), and loamy sand (C) have shown that SiO_2 and silicon-aluminous predominate in their structure (Fig. 2).

Diffraction peaks appearing in 2θ° = 20.8°, 27.2°, 50.7°, and 60.1° can be readily indexed to a pure α-Quartz SiO_2 phase [25]. Quartz is the dominant phase in sandy loam (A), loam (B), and loamy sand (C), with contents of 48.2, 60.9, and 57.4 wt.%, respectively. It is evident that sample B differs from A and C, which is manifested by a more intense peak for kaolinite (2θ = 12.2), and a less intense peak for Christobalite beta (2θ = 19.9) and microclines (2θ = 28.1). In addition, sample B did not detect potassium iron silicate (P) while in spectrum of A and C bands at 2θ = 13.76 and 28.72 reflects the presence of this [26].

The similarity between materials A and C is obvious, but the higher intensity of the characteristic quartz (2θ = 27.2) and microcline peak (2θ = 28.1) for sample C can be pointed out.

The results of textural, structural, and semi-quantitative analysis of selected samples are summarized in Table 2.

3.1.2. FTIR analysis

The FTIR spectra obtained for samples A, B, and C are shown in Fig. 3.

The OH stretching vibrations of the Si–OH group absorb in the same region as alcohols, 3,700–3,200 cm^{-1}, and strong

Table 1
Kinetic model equations

Kinetic model	Nonlinear form	Equation	Linear form	Equation	Reference
Pseudo-first-order equation	$q_t = q_e\left(1 - e^{-k_1 t}\right)$	(3a)	$\ln\left(q_e - q_t\right) = \ln\left(q_e\right) - k_1 t$	(3b)	[21]
Pseudo-second-order equation	$q_t = \dfrac{t}{\dfrac{1}{k_2 q_e^2} + \dfrac{t}{q_e}}$	(4a)	$\dfrac{t}{q_t} = \dfrac{1}{k_2 q_e^2} + \dfrac{1}{q_e} t$	(4b)	[22]
Elovich	$q_t = \dfrac{1}{\beta}\ln\left(1 + \alpha\beta t\right)$	(5a)	$q_t = \left(\dfrac{1}{\beta}\right)\ln\left(\alpha\beta\right) + \left(\dfrac{1}{\beta}\right)\ln\left(t\right)$	(5b)	[23]
Weber–Morris (W–M)	$q_t = k_{\text{id}}\sqrt{t} + C$	(6a)	/	(6b)	[24]

q_e (μg·g^{-1}) – the amounts of metal ions adsorbed at equilibrium; q_t (μg·g^{-1}) – the amounts of metal ions adsorbed at time t in min; t (min) – the contact time; k_1 (min^{-1}) – the pseudo-first-order rate constant; k_2 (g·μg^{-1}·min^{-1}) – the pseudo-second-order rate constant; α (μg·g^{-1}·min^{-1}) – the initial adsorption rate; β (g·μg^{-1}) – the desorption constant; k_{id} (μg·g^{-1}·min$^{-1/2}$) – the intraparticle diffusion rate constant; C (μg·g^{-1}) – the constant proportional to the boundary layer thickness.

Table 2
Properties of soil samples applied as adsorbents

Sample	Constituent, wt.%	Sand %	Silt %	Clay %	Soil texture class*	Organic matter %	Particle diameter mm	Soil pH
A	Quartz (α-SiO_2), 48.2; Microcline maximum ($KAlSi_3O_8$), 32.6; Potassium iron silicate ($K_{1.11}(Fe_{1.11}Si_{0.89}O_4)$), 9.5; Christobalite beta (high) (SiO_2), 6.4; Kaolinite ($Al_2(Si_2O_5)(OH)_4$), 3.4;	69.6	26.0	4.4	Sandy loam	3.42	0.5–1.0	5.47
B	Quartz (α-SiO_2), 60.9; Kaolinite ($Al_2(Si_2O_5)(OH)_4$), 22.6; Microcline maximum ($KAlSi_3O_8$), 11.3; Sanidine Ferric ($KFe_{0.28}Al_{0.72}Si_3O_8$), 3.0; Christobalite beta (high) (SiO_2), 2.2;	43.5	34.8	21.7	Loam	4.02	<2.0	4.84
C	Quartz (α-SiO_2), 57.4; Microcline maximum ($KAlSi_3O_8$), 20.6; Kaolinite ($Al_2(Si_2O_5)(OH)_4$), 4.9; Christobalite beta (high) (SiO_2), 8.7; Potassium iron silicate ($K_{1.11}(Fe_{1.11}Si_{0.89}O_4)$), 8.4.	82.0	12.0	6.0	Loamy sand	/	<2.0	6.70

*Referred to the USDA Standard (Fig. 1).

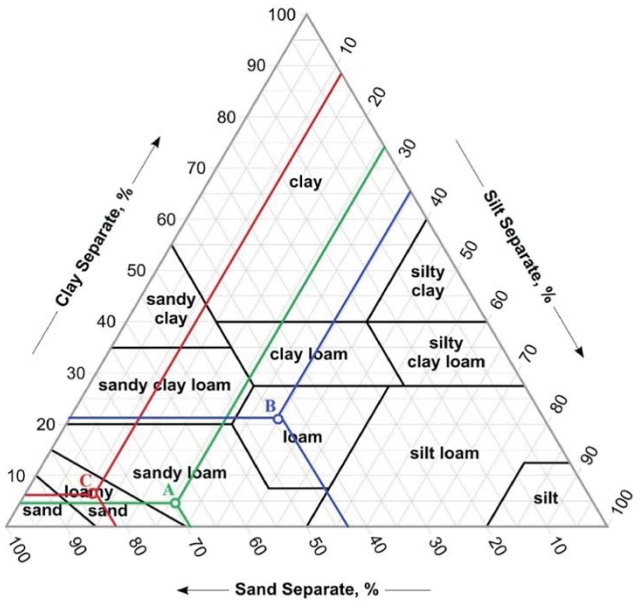

Fig. 1. Examined soils located on the USDA texture triangle.

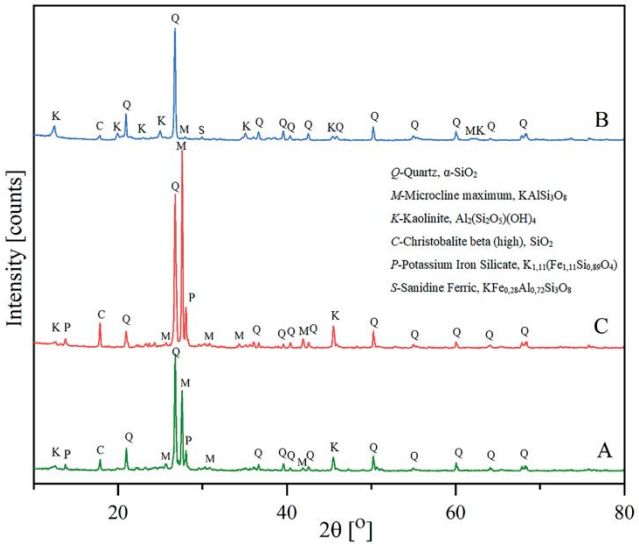

Fig. 2. The XRD patterns of the main mineral composition of tasted samples A, B, and C.

Si–O bands are at 830–1,110 cm^{-1} [27]. FT-IR spectrum of samples shows bands at 3,694 and 3,621 cm^{-1}; they correspond to the stretching –OH groups of clay mineral structure [28]. The difference in intensity is a consequence of different clay content: sample B has the greatest intensity for these bands and the highest clay content.

The characteristic of infrared bands associated with quartz crystals is in the range of 1,200–400 cm^{-1} [29]. Bands at 1,025–912 cm^{-1} correspond to the stretching vibrations of the Si–O mineral group [27,30]. Absorptions between 795 and 752 cm^{-1} are due to quartz [31]. The peak at 695 cm^{-1} can be assigned to symmetrical bending vibration of the Si–O group. Bands at 535 (Si–O) and 465 cm^{-1} (Si–O) are characteristics of kaolinite [32]. The IR band at 624 cm^{-1} identified in the spectra of samples A and C can be assigned to Fe–O stretching vibration [33].

3.1.3. SEM analysis

The surface morphology micrographs of samples A, B, and C determined by SEM are shown in Fig. 4.

SEM analysis showed that particles' morphology was not uniform, particles were tightly aggregated, and their

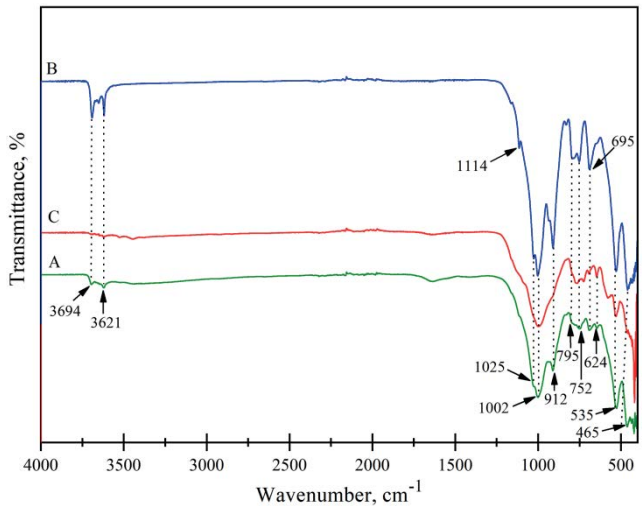

Fig. 3. FTIR spectra of sandy loam (A), loam (B), and loamy sand (C).

size ranged from sub-micrometers to a few micrometers. The surface morphology of the studied mineral samples was very complex due to the uneven shape of the particles. The morphology of sample A, sandy loam (Fig. 4a, 20 μm), consists of a significant number of crystals of different sizes, where small crystals (with a diameter less than 5 μm) have irregular geometric shapes such as a spherical hexagon and pseudo-hexagonal particles. In Fig. 4a (5 μm), a large aggregate of a hexagonal but irregular shape can be observed. In material B (loam), the large particle size presents kaolinite "booklets" (leaf-like particles formation on their surface), the micron-morphological structures consisting of platelets that is characteristic of kaolinite [34]. Fig. 4b shows different sizes of irregular loam surface structure (B). Large crystals (>10 μm) usually form booklets composed of pseudo-hexagonal merged plates, while small crystals (<2.5 μm) appear as pseudo-hexagonal single platelets [35]. On the rough hard-packed surface of the sample C (Fig. 4c), particles stick together in large uniform masses. Loamy sand (C) shows the lowest self-agglomeration

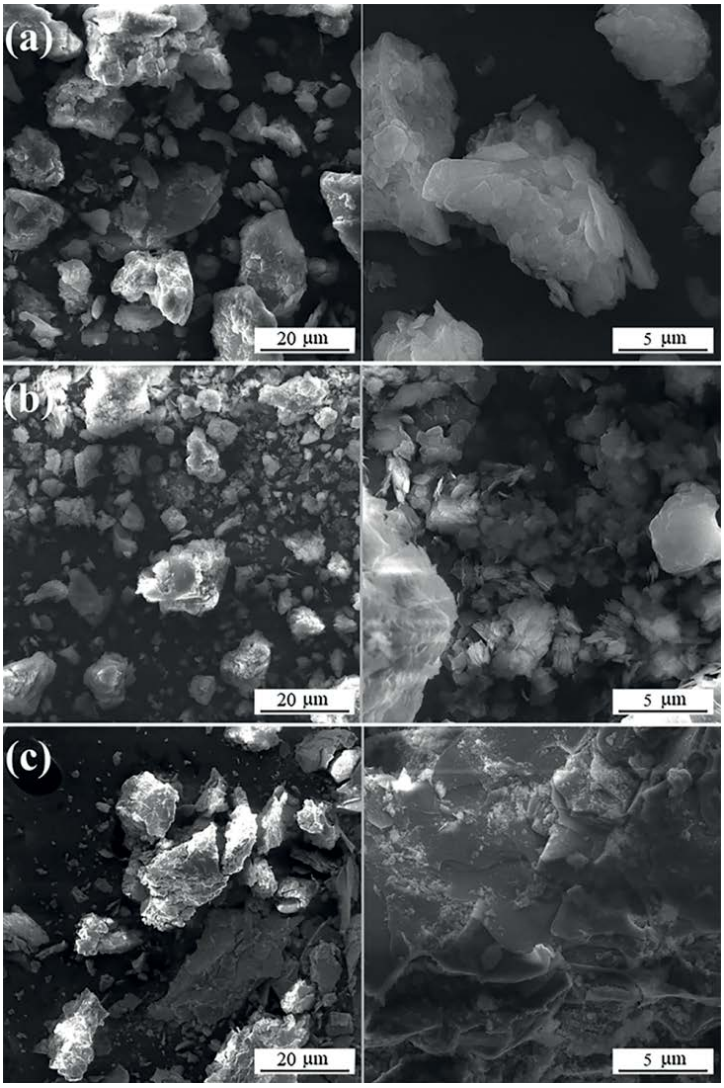

Fig. 4. SEM images of soil samples: (a) sandy loam (A), (b) loam (B), and (c) loamy sand (C).

compared to other materials where significant particle agglomeration was observed, especially for loam (B).

3.1.4. BET analysis

Properties of samples A, B, and C as a result of BET analysis are shown in Table 3. Samples A and B have significantly higher accessibility of surface sites (higher V_{meso}) than sample C, which could contribute to the higher efficiency of removing heavy metals from aquatic solutions. The very low porosity (macropores) of sample C could result from a rough soil surface, as shown in Fig. 4c (SEM).

3.2. Adsorption process optimization

Adsorption of selected heavy metals by sandy loam (A), loam (B), and loamy sand (C) has been studied using an equilibrium batch technique. All experimental conditions were selected to reduce secondary pollution; solution volume was 10 mL, the mass of adsorbent was 10 mg, and initial concentrations of lead and arsenic were 100 μg·L^{-1}. Furthermore, the application of ICP-MS, a method for low element concentration measurement, enabled the utilization of less concentrated sample solutions and, consequently, the lower solution volume, thus minimizing the negative influence on the environment during the experimental study.

3.2.1. Influence of adsorbent mass

Fig. 5 depicts the effect of adsorbent dosage on As(V) and Pb(II) adsorption on mineral materials.

Fig. 5 shows that the adsorption efficiency of the analyzed ions is typically increased with the increase in adsorbents dosage from 5 mg/10 mL to 10 mg/10 mL when it reaches the plateau. The increase in removal efficiency with adsorbent dosage could be attributed to the increasing number of active sites available for heavy metal ions adsorption [36].

The efficiency of examined soils for arsenate removal decreased in the order A > B > C. The activity of arsenic in the soil solution is controlled by the reactions of retention and release along the surfaces of Fe, Mn, and Al oxides and hydroxides [37,38]. It was demonstrated previously that Californian soils having a more significant percentage of clay and appreciable quantities of Fe oxides had a greater As retention capacity [39].

In the case of lead removal, the order is B > A > C. Each soil constituent exhibits a specific rate and binding strength affinity to retain a chemical from the aquatic phase, which could vary by changing the ambient soil circumstances [40]. Ingredients of the soil that mostly influence its behavior as lead adsorbent are clay and organic matter [41]. The higher affinity of Pb(II) ions for material B could result from a significantly higher proportion of clay

Table 3
The textural properties of the tested samples

Parameters	Sandy loam (A)	Loam (B)	Loamy sand (C)
Specific surface, S_p, m^2·g^{-1}	3.17	7.53	0.015
Total pore volume, V_{total}, cm^3·g^{-1}	0.0108	0.0230	0.0002
Volume of mesopores, V_{meso}, cm^3·g^{-1}	0.0098	0.0216	n.m.
Mean pore diameter, D_{sr}, nm	19.82	13.07	n.m.

n.m. the porosity could not be measured.

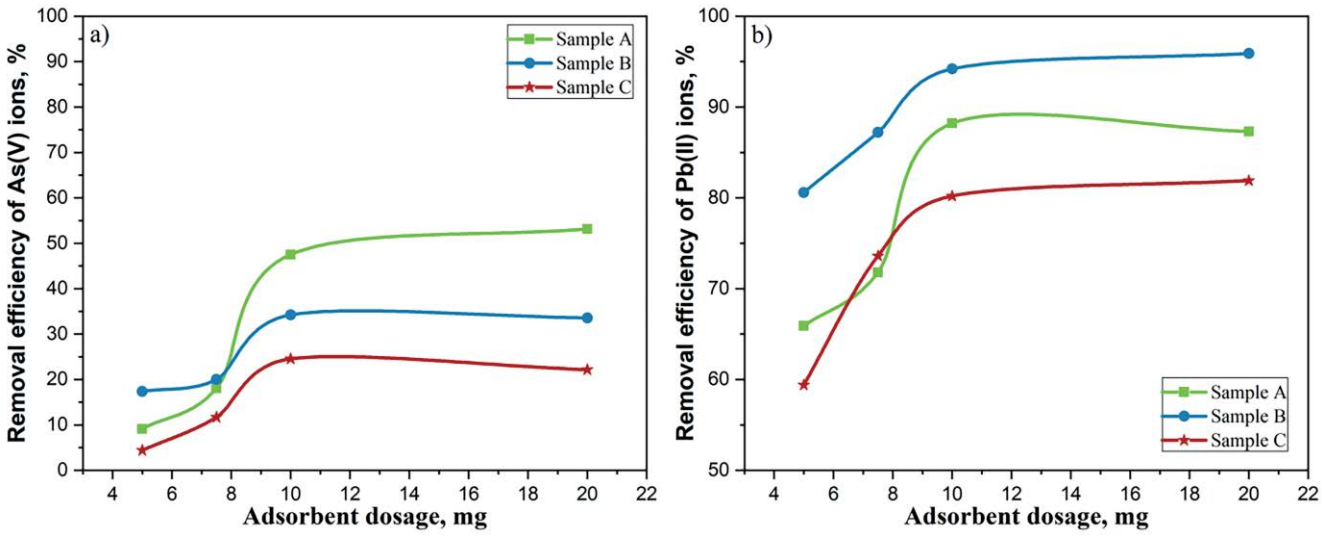

Fig. 5. Removal of As(V) and Pb(II) ions from aqueous solutions using different adsorbent masses (C_i = 100 μg·L^{-1}, pH$_i$(As(V)) = 6, pH$_i$(Pb(II)) = 5, T = 25°C and t = 24 h).

(almost five times more) and a slightly higher organic matter content than material A.

For both ions, the lowest results were obtained with material C, which was expected taking into account its characteristics (textural and structural), low specific surface (0.015 $m^2 \cdot g^{-1}$), and the fact that it does not contain organic matter, which is significant for Pb adsorption.

3.2.2. *Influence of pH*

The pH value significantly affects the speciation of pollutant ions and surface functional groups capable of attracting/binding pollutants. The effect of pH on As(V) and Pb(II) removal by soil samples was analyzed at pH 4, 5, and 6. In the selected pH range, tested pollutants are dominantly presented in one form, Pb(II) as Pb^{2+} ion, and As(V) as oxyanion, $H_2AsO_4^-$. Moreover, in experiments under these pH values, the generation of highly acidic or highly alkaline waste has been avoided.

The As(V) and Pb(II) ions speciation were performed using Visual Minteq 3.1 software version and are shown in Fig. 6.

Fig. 7 presents the effect of initial solution pH on As(V) and Pb(II) adsorption by examined soil samples. Preliminary experiments revealed that 24 h was sufficient to reach sorption equilibrium.

It can be noticed that Pb(II) removal efficiency is higher than 80% for all tested materials at all examined pH values, indicating their potential application as adsorbents of this heavy metal from water and soil. On the other hand, the most effective material for As(V) removal in the whole tested pH range was sandy loam (A), although the efficiency of material B was not negligible, either.

The obtained results indicate that at the examined pH values, sandy loam (A) and loam (B) have a high affinity for

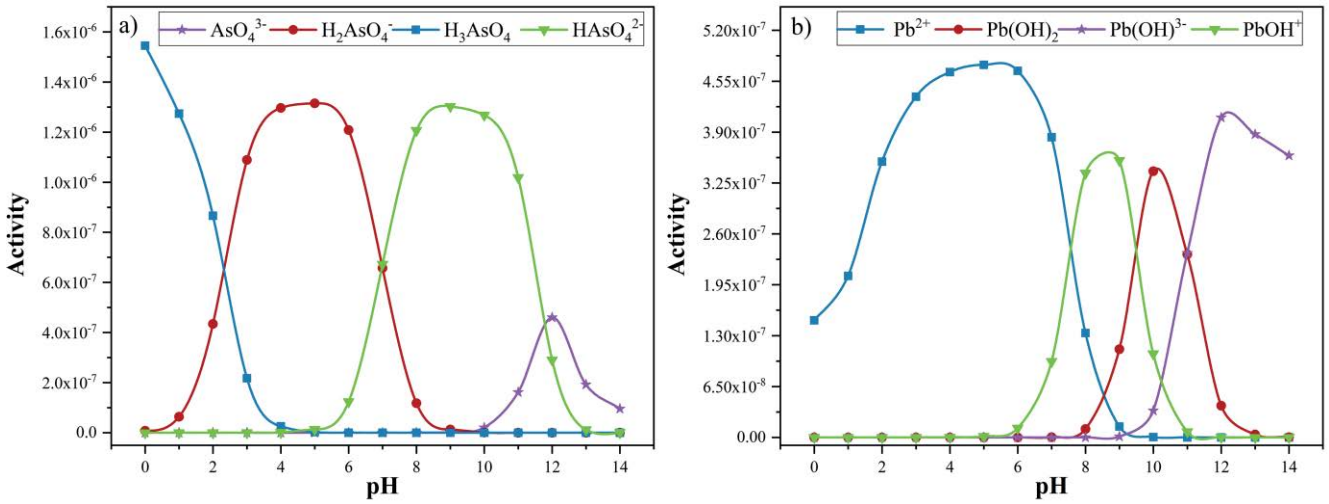

Fig. 6. Theoretical prediction of arsenic and lead species using Visual Minteq 3.1 software.

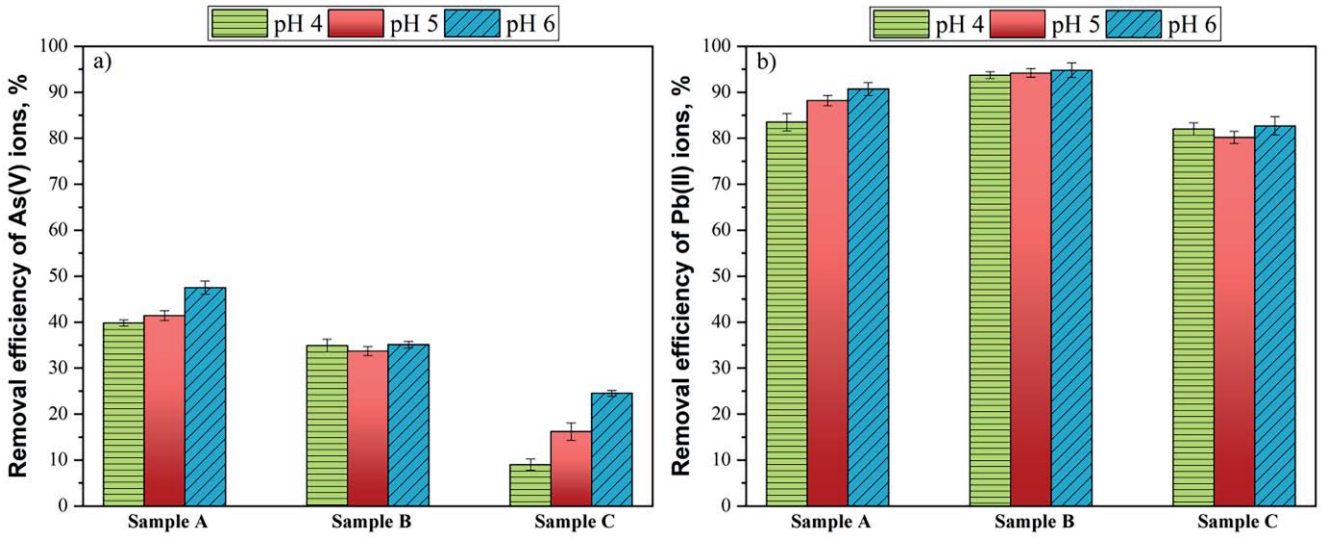

Fig. 7. Effect of pH on arsenic and lead adsorption from single ion solution by sandy loam (A), loam (B), and loamy sand (C); experimental conditions: initial concentration 100 $\mu g \cdot L^{-1}$, adsorbent dosage 10 mg, solution volume 10 mL, room temperature (25°C).

selected heavy metals in cationic/anionic form in an aqueous solution. In addition, the mobility of Pb(II) and As(V) in these acidic soils (Table 2) is reduced, especially in the case of lead, providing a reduced possibility of underground water pollution.

3.3. Kinetic results

Adsorption relates to the sorbent's physicochemical characteristics experimental conditions (temperature, pH values, hydrodynamic conditions, contact time) [42]. Generally, the adsorption process could be comprised of either one or more steps depending on the number of parameters that affect the reaction, as well as the complexity of the adsorption process [43]. Adsorption of species on a solid surface follows three steps: (i) transport of the adsorbate (ions in case of solutions) from the bulk to the external surface of the adsorbent, (ii) passage through the liquid film attached to the solid surface, and (iii) interactions with the surface atoms of the solid leading to chemisorption or weak adsorption. The slowest step determines the total rate of interactions and the kinetics of the adsorption process [44].

A very high initial rate of heavy metal sorption has been observed (Fig. 8); for lead, even 75% was sorbed in the first 100 min. Prolonged contact time did not lead to significant separation of lead or arsenic. Similar results were obtained by [45].

In order to evaluate the adsorption of Pb(II) and As(V), kinetic models such as the pseudo-first-order, pseudo-second-order, and Elovich equation were applied. Since these models cannot identify in which step the speed is controlled, it was necessary to apply the Weber-Morris diffusion model [46].

The parameters obtained from kinetic equations are shown in Table 4.

The best correlation was obtained for the pseudo-second-order model followed by the Weber-Morris diffusion model (Fig. 9). Namely, according to the regression coefficients, R^2, it was indicated that the pseudo-second-order theory was the most suitable for describing the adsorption of Pb(II) and As(V) ions on the surface of the applied materials (sandy loam, A; loam, B and loamy sand, C). Studies have shown that adsorption that fits the pseudo-second-order model well often can be explained by diffusion-based mechanisms [47].

Ho and McKay's second-order model assume that sharing electrons through chemisorption controls the adsorption rate. It is known that chemisorption is a rather slow process and takes a long time to establish equilibrium. For lead and arsenic, very fast adsorption was observed in the first stage indicating physical sorption.

In the Weber-Morris diffusion model (W-M), the plot q_t vs. $t^{1/2}$ yields a straight line that passes through the origin when the adsorption process depends on intraparticle diffusion. In the examined case, the plots for As(V) and Pb(II) for all materials do not pass through the origin (zero intercepts), which indicates that intraparticle diffusion was not the only rate-limiting step [48,49].

The result of W-M fitting (Fig. 9) shows that for both heavy metals, the adsorption process can be described through two stages: (1) fast kinetics in the first stage and (2) very slow attainment of equilibrium in the second-stage. The first stage, which might be attributable to external surface adsorption, had a significantly higher adsorption rate than the second-step, which could be viewed as an intraparticle diffusion into micro-pores and mesopores of the adsorbent, thereby decreasing the adsorption rate. The intraparticle diffusion stage controls and limits the rate of adsorption [50]. This fact is also indicated by the parameters of the W-M model (Table 4), where the value of constant k_{id1} (phase 1) is higher than the value of k_{id2} (phase 2) for As(V) as well as for Pb(II), which means that the external surface adsorption was much faster than the intraparticle diffusion. In the first stage, the kinetics of adsorption for both heavy metals are significantly faster, probably due to a large number of available sites on the adsorbent, while the second-stage is characterized by the slower diffusion transport within the

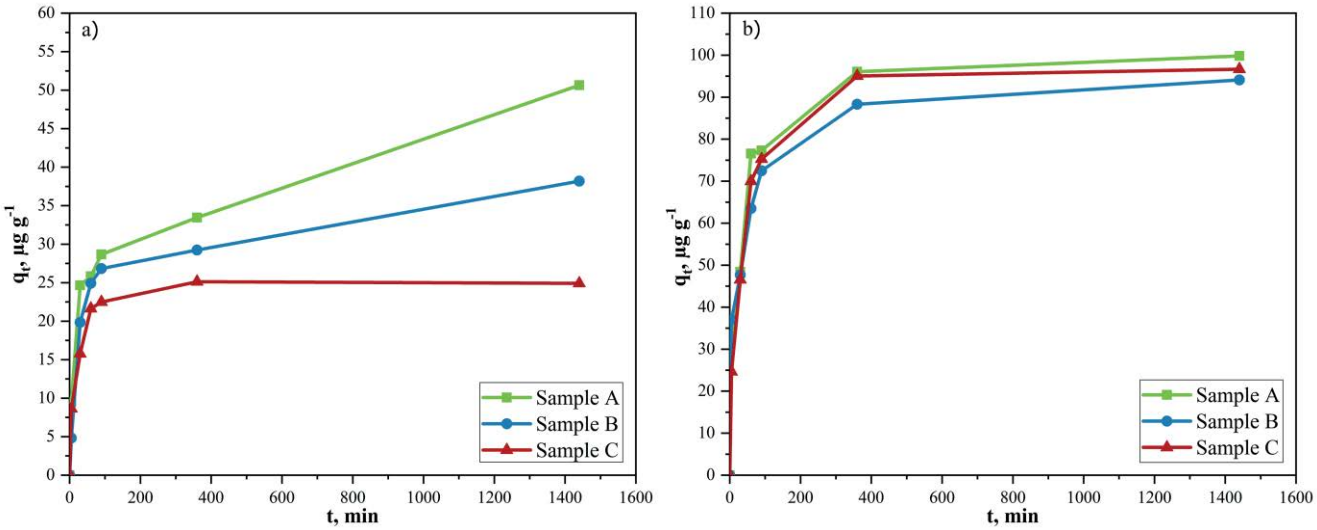

Fig. 8. Sorption kinetics of As(V) – left and Pb(II) – right, on sandy loam (A), loam (B), and loamy sand (C).

porous system ($k_{id1} > k_{id2}$) [51]. Also, the intercept C_2 of the second-stage (W-M 2) has a higher value compared to the first stage, C_1 (W-M 1), which is an indication of a thicker boundary; thus the higher resistance in stage two, stemming from the intraparticle diffusion [51,52].

Comparing the natural samples treated in this study with those collected from the literature offers valuable information on their adsorption performances. The differences in the experimental conditions were significant due to the variety of materials used (Tables 5 and 6).

Most of the research (Tables 5 and 6) has described singular removal of As(V) and Pb(II) ions by adsorption onto natural sorbents with different percentages of sand, clay, and silt in their structure. In this study, the best kinetic correlation was the pseudo-second-order (PSO) model regarding both examined ions obtained in previous studies (Tables 5 and 6).

Also, the adsorption was performed from concentrated solutions (most of them in mg·L^{-1}), and the residual ion concentrations were measured using AAS or ICP-OES instrumental technique. Nevertheless, even low levels of metal ion concentration (expressed in μg·L^{-1}) in the aqueous system pose a risk to water safety and human health. Therefore, the experiments in this work were performed with lower initial metal ion concentrations (0.1 mg·L^{-1}) compared to the other studies (0.05–100 mg·L^{-1} for As(V) and 20–1,000 mg·L^{-1} for Pb(II), respectively) and ICP-MS technique has been applied. Using lower concentrations of

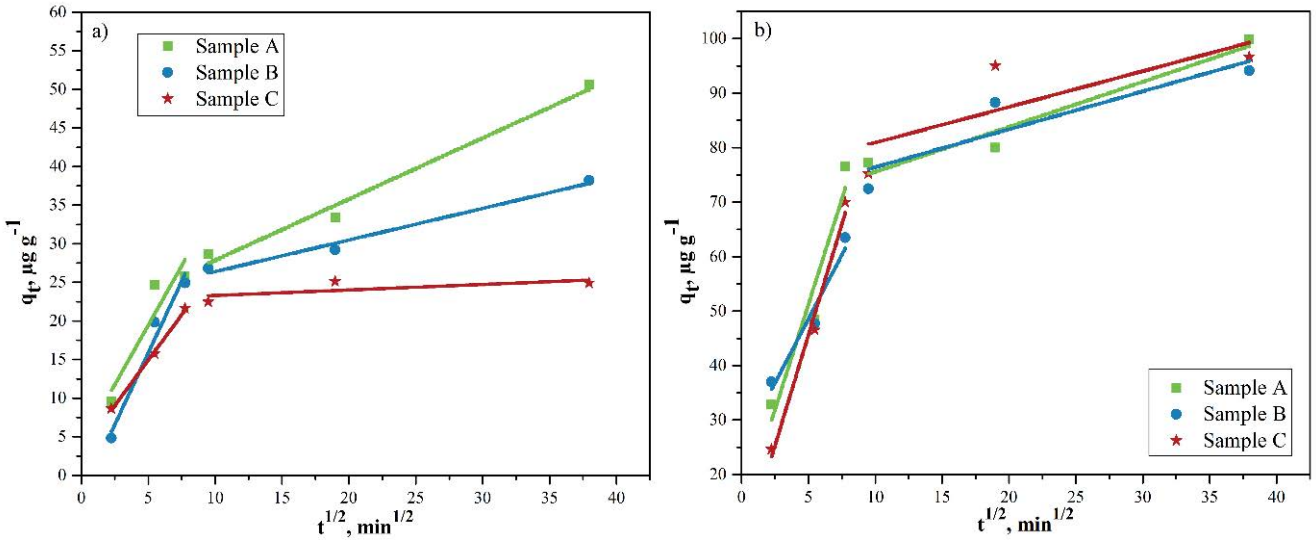

Fig. 9. Experimental data for As(V) (up) and Pb(II) sorption (down) onto examined soils fitted to the Weber–Morris model.

Table 4
Kinetic parameters for the adsorption of As(V) and Pb(II) onto natural-based material using different models

General kinetic models	Parameters	Sandy loam (A)		Loam (B)		Loamy sand (C)	
		As(V)	Pb(II)	As(V)	Pb(II)	As(V)	Pb(II)
Pseudo-first-order equation	k_1 (min^{-1})	0.002	0.008	0.088	1.648	0.838	0.177
	q_e (μg g^{-1})	30.46	53.22	30.84	39.89	32.42	173.6
	R^2	0.6338	0.9435	0.7424	0.7897	0.3152	0.6787
Pseudo-second-order equation	k_2 (g·μg^{-1}·min^{-1})	0.000	0.000	0.003	0.004	0.004	0.005
	q_e (μg g^{-1})	52.10	101.36	39.05	95.65	25.13	98.33
	R^2	0.9863	0.9998	0.996	0.9998	0.9999	0.9998
Elovich	α (μg·g^{-1}·min$^{-1/2}$)	0.078	0.194	0.067	0.262	0.352	0.109
	β (μg g^{-1})	11.26	16.15	13.62	18.69	25.19	15.11
	R^2	0.953	0.9092	0.9374	0.9473	0.8306	0.9203
Intraparticle diffusion kinetic model constant: W-M (step 1)	k_{id1} (μg·g^{-1}·min$^{-1/2}$)	3.077	7.729	3.717	8.128	2.348	4.704
	C_1 (μg g^{-1})	4.143	12.76	2.625	5.179	3.246	25.15
	R^2	0.8778	0.931	0.9693	0.9854	0.9978	0.9554
W-M (step 2)	k_{id2} (μg·g^{-1}·min$^{-1/2}$)	0.7915	0.8275	0.4096	0.6961	0.0715	0.6564
	C_2 (μg g^{-1})	20.07	67.39	22.35	69.55	22.59	74.45
	R^2	0.9844	0.9509	0.9828	0.8095	0.4968	0.6379

Table 5
The review of literature data on the adsorption characteristics of As(V) on natural materials

Soil characteristics							Adsorption characteristics								Reference
Soil texture class	Sand %	Silt %	Clay %	Organic matter %	pH	FTIR/XRD (Fe content)	Mass of adsorbent (m_{ads}), g	Volume (V), mL	Initial concentration (C_i), mg·L^{-1}	Initial pH$_i$	Reaction time (t), h	Adsorption capacity (q_e), μg·g^{-1}	Kinetic model	Analytical technique	
Sandy loam	56	35.5	8.5	1.53	7.02	/	0.6	150	0.09	9.5	72	10.46	PSO	AAS	[53]
Loamy sand	56.7	23.6	19.7	3.9	7.6	/	3	30	0–100	/	24	250	/		
Sandy loam	79.5	15.3	5.2	0.8	7.3	/	3	30	0–100	/	24	900	/	HG-AFS	[54]
Sandy soil	98.1	1.0	0.9	0.7	6.4	/	3	30	0–100	/	24	80	/		
Sandy soil	84.07	2.01	13.92	/	5.26	/	1.25	50	0–75	5	96	1,250	/	ICP-MS	[55]
Sandy loam	59.01	24.49	17.5	/	7.3	/	0.02	5	0.04	/	2	13.22	/	AFS	[56]
Loam	/	/	/	1.62	8	FTIR: Fe–O	0.5	100	0.1	3	0–120	30.1	PSO	AAS	[20]
Sandy loam	/	/	/	1.03	8.4	FTIR: Fe–O	0.5	100	0.1	3	0–120	27.5	PSO		
Clay loam	43.04	19.68	37.28	2.7	7.33	XRD: Fe_2O_3	10	500	7.5–75	/	1	93.8	PSO	ICP-OES	[57]
Silty clay loam	23.2	50.3	26.5	/	6.49	FTIR: Si–O–Fe	0.5	20	0.05	6.2	0.3–30	479.2	/	ICP-MS	[58]
Sandy soil	92.5	2.3	5.2	2.4	7.7	/	25	250	0.5	7	4–144	4.85	PSO	GF-AAS	[59]
Sandy loam (A)	69.6	26.0	4.4	3.42	5.47	FTIR: Fe–O XRD: $K_{1.11}(Fe_{1.11}Si_{0.89}O_4$	0.01	10	0.1	6	0–24	52.1	PSO	ICP-MS	This study
Loam (B)	43.5	34.8	21.7	4.02	4.84	/	0.01	10	0.1	6	0–24	39.0	PSO	ICP-MS	This study
Loamy sand (C)	82.0	12.0	6.0	/	6.7	FTIR: Fe–O XRD: $K_{1.11}(Fe_{1.11}Si_{0.89}O_4$	0.01	10	0.1	6	0–24	25.1	PSO	ICP-MS	This study

Table 6
The review of literature data on the adsorption characteristics of Pb(II) on natural materials

Soil characteristics						Adsorption characteristics								Reference
Soil texture class	Sand %	Silt %	Clay %	Organic matter %	pH	Mass of adsorbent (m_{ads}), g	Volume (V), mL	Initial concentration (C_i), mg·L^{-1}	Initial pH$_i$	Reaction time (t), h	Adsorption capacity (q_e), μg·g^{-1}	Kinetic model	Analytical technique	
Sandy soil	/	/	/	0.15	/	2	20	0–1,000	7.78	24	2,100	/	AAS	[60]
Sandy soil	92	6	2	1.4	3.97	10	200	20–100	5	/	1,000	PSO	ICP-OES	[61]
Sandy loam	80.10	8.45	11.45	1.85	5.97	5	50	0–50	/	1	24,390	/	AAS	[62]
Sandy loam	55.25	31.91	14.07	0.896	7.52	0.2	20	20	7	3	25,070	PSO	AAS	[63]
Sandy soil	94	5.3	0.7	0.2	5.3	2.5	1,500	100	/	72	1,069.5	PFO	AAS	[64]
Sandy loam	76.4	6	15	0.56	7.4	0.10	20	50–250	3–11	0.3–1	27,600	PSO	AAS	[65]
Loamy sand	76	12.76	11	0.479	5.8	0.10	20	50–250	3–11	0.3–1	26,350	PSO	AAS	[65]
Loamy sand	81	9.1	3.08	/	6.5	2.0	50	25	2–8	0–1.5	647	PSO	AAS	[66]
Sandy loam (A)	69.6	26.0	4.4	3.42	5.47	0.01	10	0.1	5	0–24	101.4	PSO	ICP-MS	This study
Loam (B)	43.5	34.8	21.7	4.02	4.84	0.01	10	0.1	5	0–24	95.6	PSO	ICP-MS	This study
Loamy sand (C)	82.0	12.0	6.0	/	6.7	0.01	10	0.1	5	0–24	98.3	PSO	ICP-MS	This study

chemicals reduces additional environmental pollution and thus, respects and follows the concept of green chemistry and sustainable development.

4. Conclusion

This paper presents the results of an environmentally sustainable application of natural raw materials, with disparate soil textures, for the adsorption of As(V) and Pb(II) from an aqueous environment. Sandy loam (A), loam (B), and loamy sand (C) with different semi-quantitative compositions and structures have been studied for the removal of heavy metal ions. Comprehensive structural analysis has shown that the main mineral constituents of all three materials were silicates, quartz, and calcite. Based on the optimal experimental conditions, the results for the efficiency of selected ions removal have shown the following trend of material adsorption affinity:

- As(V) separation – A (47.5%) > B (34.2%) > C (24.5%);
- Pb(II) separation – B (94.2%) >A (88.2%) > C (80.2%).

The obtained results indicate that materials A and B could be potentially used as low-cost adsorbents, especially in the relatively low initial concentration (100 $\mu g \cdot L^{-1}$) of examined pollutants. The adsorption was very efficient within the initial hundred minutes, with 75% of lead and 35% of arsenate removal, indicating that used natural materials under examined experimental conditions could provide an alternative environmentally sustainable solution for pollutants separation. The encouraging results obtained in this paper will present the basis for further research directed towards material modification, pollutant separation from multi-elemental solutions, and soil and heavy metal separation from water in flow systems.

Funding information

This work was supported by the Ministry of Education, Science and Technological Development of the Republic of Serbia (Contract Nos. 451-03-9/2022-14/200135, 451-03-9/2022-14/200287 and 451-03-68/2022-14/200017).

References

[1] K. Pantić, Z.J. Bajić, Z.S. Veličković, V.R. Djokić, J.D. Rusmirović, A.D. Marinković, A.A. Perić-Grujić, Adsorption performances of branched aminated waste polyacrylonitrile fibers: experimental versus modelling study, Desal. Water Treat., 171 (2019) 223–249.
[2] Renu, M. Agarwal, K. Singh, Heavy metal removal from wastewater using various adsorbents: a review, J. Water Reuse Desal., 7 (2017) 387–419.
[3] S. Mihajlović, M. Vukčević, B. Pejić, A.P. Grujić, M. Ristić, Application of waste cotton yarn as adsorbent of heavy metal ions from single and mixed solutions, Environ. Sci. Pollut. Res., 27 (2020) 35769–35781.
[4] A. Das, N. Bar, S.K. Das, Adsorptive removal of Pb(II) ion on *Arachis hypogaea*'s shell: batch experiments, statistical, and GA modeling, Int. J. Environ. Sci. Technol., (2022), doi: 10.1007/s13762-021-03842-w.
[5] M. Ghorbani, O. Seyedin, M. Aghamohammadhassan, Adsorptive removal of lead(II) ion from water and wastewater media using carbon-based nanomaterials as unique sorbents: a review, J. Environ. Manage., 254 (2020) 109814.
[6] A. Das, N. Bar, S.K. Das, Pb(II) adsorption from aqueous solution by nutshells, green adsorbent: adsorption studies, regeneration studies, scale-up design, its effect on biological indicator and MLR modeling, J. Colloid Interface Sci., 580 (2020) 245–255.
[7] T. Mitra, N. Bar, S.K. Das, Rice husk: green adsorbent for Pb(II) and Cr(VI) removal from aqueous solution—column study and GA–NN modeling, SN Appl. Sci., 1 (2019) 5.
[8] S. Gu, X. Kang, L. Wang, E. Lichtfouse, C. Wang, Clay mineral adsorbents for heavy metal removal from wastewater: a review, Environ. Chem. Lett., 17 (2019) 629–654.
[9] H. Zeng, L. Zhai, T. Qiao, Y. Yu, J. Zhang, D. Li, Efficient removal of As(V) from aqueous media by magnetic nanoparticles prepared with iron-containing water treatment residuals, Sci. Rep.-UK, 10 (2020) 1–12.
[10] M.F. Hamza, S. Lu, K.A.M. Salih, H. Mira, A.S. Dhmees, T. Fujita, Y. Wei, Th. Vincent, E. Guibal, As(V) sorption from aqueous solutions using quaternized algal/polyethyleneimine composite beads, Sci. Total Environ., 719 (2020) 1–11.
[11] U.S. Environmental Protection Agency (USEPA), National Primary Drinking Water Regulations. Available at: https://www.epa.gov/ground-water-and-drinking-water/national-primary-drinking-water-regulations (The Last Access: 27.07.2022.)
[12] World Health Organization (WHO), Guidelines for Drinking-Water Quality: Fourth Edition Incorporating the First Addendum, World Health Organization, Geneva (Licence: CC BY-NC-SA 3.0 IGO), 2017.
[13] C.P.J. Isaac, A. Sivakumar, Removal of lead and cadmium ions from water using Annona squamosa shell: kinetic and equilibrium studies, Desal. Water Treat., 51 (2013) 7700–7709.
[14] C.F. Carolin, P.S. Kumar, A. Saravanan, G.J. Joshiba, M. Naushad, Efficient techniques for the removal of toxic heavy metals from aquatic environment: a review, J. Environ. Chem. Eng., 5 (2017) 2782–2799.
[15] S. Mahdavi, M. Jalali, A. Afkhami, Removal of heavy metals from aqueous solutions using Fe_3O_4, ZnO, and CuO nanoparticles, J. Nanopart. Res., 14 (2012) 846.
[16] M.B. Đolić, V.N. Rajaković-Ognjenović, J.P. Marković, J.P. Marković, Lj.J. Janković-Madić, M.N. Mitrić, A.E. Onjia, Lj.V. Rajaković, The effect of different extractants on lead desorption from a natural mineral, Appl. Surf. Sci., 324 (2015) 221–231.
[17] A.A. Alghamdi, A.B. Al-Odayni, W.S. Saeed, A. Al-Kahtani, F.A. Alharthi, T. Aouak, Efficient adsorption of lead(II) from aqueous phase solutions using polypyrrole-based activated carbon, Materials (Basel), 12 (2019) 2–16.
[18] B.O. Otunola, O.O. Ololade, A review on the application of clay minerals as heavy metal adsorbents for remediation purposes, Environ. Technol. Innov., 18 (2020) 100692.
[19] M. Alamgir, In: Environmental Remediation Technologies for Metal-Contaminated Soils, The Effects of Soil Properties to the Extent of Soil Contamination with Metals, 2017, pp. 1–20.
[20] A.P. Rawat, V. Kumar, P. Singh, A.C. Shukla, D.P. Singh, Kinetic behavior and mechanism of arsenate adsorption by loam and sandy loam soil, Soil Sediment Contam., 31 (2022) 15–39.
[21] S. Lagergren, Zur theorieder sogennanten adsorption geloester stoffe, kungliga svenska vetenskapsakademiens, Handlingar, 24 (1898) 1–39.
[22] Y.S. Ho, G. McKay, Pseudo-second-order model for sorption processes, Process Biochem., 34 (1999) 451–465.
[23] S.Y. Elovich, O.G. Larinov, Theory of Adsorption from Solutions of Non Electrolytes on Solid (I) Equation Adsorption from Solutions and the Analysis of Its Simplest Form, (II) Verification of the Equation of Adsorption Isotherm from Solutions, Izv. Akad. Nauk. SSSR, Otd. Khimicheskikh Nauk, 2 (1962) 209–216.
[24] W.J. Weber, J.C. Morris, Kinetics of adsorption on carbon from solutions, J. Sanit. Eng. Div. Am. Soc. Civ. Eng., 89 (1963) 31–60.
[25] B. Fonseca, H. Figueiredo, J. Rodrigues, A. Queiroz, T. Tavares: Mobility of Cr, Pb, Cd, Cu and Zn in a loamy sand soil: a comparative study, Geoderma, 164 (2011) 232–237.
[26] W.A. Dollase, C.R. Ross, Crystal structures of the body-centered tetragonal tectosilicates: $K_{1.14}Mg_{0.57}Si_{1.43}O_4$, $K_{1.10}Zn_{0.55}Si_{1.45}O_4$, and $K_{1.11}Fe^3{}_{1.11}Si_{0.89}O_4$, Am. Mineral., 78 (1993) 627–632.

[27] R.M. Silverstein, F.X. Webster, D.J. Kiemle, In: Spectrometric Identification of Organic Compounds 7th ed., 2005.
[28] P.G. Rouxhet, N. Samudacheata, H. Jacobs, O. Anton, Attribution of the OH stretching bands of kaolinite, Clay Miner., 12 (1977) 171–179.
[29] J. Gadsden, The infrared spectra of minerals and related inorganic compounds, Mineral. Mag., 40 (1975) 540.
[30] M.E. Parolo, M.C. Savini, R.M. Loewy, Characterization of soil organic matter by FT-IR spectroscopy and its relationship with chlorpyrifos sorption, J. Environ. Manage., 196 (2017) 316–322.
[31] F. Le Guillou, W. Wetterlind, R.A. Viscarra Rossel, W. Hicks, M. Grundy, S. Tuomi, How does grinding affect the mid-infrared spectra of soil and their multivariate calibrations to texture and organic carbon?, Soil Res., 53 (2015) 913–921.
[32] M. Alkan, Ö. Demirbaş, M. Doğan, Electrokinetic properties of kaolinite in mono- and multivalent electrolyte solutions, Microporous Mesoporous Mater., 83 (2005) 51–59.
[33] M. Gotić, S. Musić, Mossbauer, FT-IR and FE SEM investigation of iron oxides precipitated from $FeSO_4$ solutions, J. Mol. Struct., 834–836 (2007) 445–453.
[34] E. Balan, G. Calas, D.L. Bish, Kaolin-group minerals: from hydrogen-bonded layers to environmental recorders, Elements, 10 (2014) 183–188.
[35] M. Ivanić, N. Vdović, S. de B. Barreto, V. Bermanec, I. Sondi, Mineralogy, surface properties and electrokinetic behaviour of kaolin clays derived from naturally occurring pegmatite and granite deposits, Geol. Croat., 68 (2015) 139–145.
[36] F. Sharifipour, S. Hojati, A. Landi, A. Faz Cano, Kinetics and thermodynamics of lead adsorption from aqueous solutions onto Iranian sepiolite and zeolite, Int. J. Environ. Res., 9 (2015) 1001–1010.
[37] N. Livesey, P. Huang, Adsorption of arsenate by soils and its relation to selected chemical properties and anions, Soil Sci., 131 (1981) 88–94.
[38] K. De Brouwere, E. Smolders, R. Merckx, Soil properties affecting solid-liquid distribution of As(V) in soils, Eur. J. Soil Sci., 55 (2004) 165–173.
[39] B.A. Manning, S. Goldberg, Arsenic(III) and arsenic(V) adsorption on three California soils, Soil Sci., 162 (1997) 886–895.
[40] T.A. Elbana, H. Magdi Selim, Multireaction modeling of lead(Pb) and copper(Cu) sorption/desorption kinetics in different soils, Soil Syst., 3 (2019) 1–13.
[41] K.S. Lee, H.Y. Shim, D.S. Lee, D.Y. Chung, The fate and factors determining arsenic mobility of arsenic in soil-a review, Korean J. Soil Sci. Fertil., 48 (2015) 73–80.
[42] S.A. Chaudhry, Z. Zaidi, S.I. Siddiqui, Isotherm, kinetic and thermodynamics of arsenic adsorption onto iron-zirconium binary oxide-coated sand (IZBOCS): modelling and process optimization, J. Mol. Liq., 229 (2017) 230–240.
[43] Z. Veličković, G.D. Vuković, A.D. Marinković, M.S. Moldovan, A.A. Perić-Grujić, P.S. Uskoković, M.D. Ristić, Adsorption of arsenate on iron(III) oxide coated ethylenediamine functionalized multiwall carbon nanotubes, Chem. Eng. J., 181–182 (2012) 174–181.
[44] S. Sen Gupta, K.G. Bhattacharyya, Kinetics of adsorption of metal ions on inorganic materials: a review, Adv. Colloid Interface Sci., 162 (2011) 39–58.
[45] D.G. Strawn, D.L. Sparks, Effects of soil organic matter on the kinetics and mechanisms of Pb(II) sorption and desorption in soil, Soil Sci. Soc. Am. J., 64 (2000) 144–156.
[46] I. Ogbu, K. Akpomie, A. Osunkunle, S. Eze, Sawdust-kaolinite composite as efficient sorbent for heavy metal ions, Bangladesh J. Sci. Ind. Res., 54 (2019) 99–110.
[47] M.A. Hubbe, S. Azizian, S. Douven, Implications of apparent pseudo-second-order adsorption kinetics onto cellulosic materials: a review, BioResources, 14 (2019) 7582–7626.
[48] L.S.G. Galindo, A.F. De Almeida Neto, M.G.C. Da Silva, M.G.A. Vieira, Removal of cadmium(II) and lead(II) ions from aqueous phase on sodic bentonite, Mater. Res., 16 (2013) 515–527.
[49] S.A. Chaudhry, T.A. Khan, I. Ali, Zirconium oxide-coated sand based batch and column adsorptive removal of arsenic from water: isotherm, kinetic and thermodynamic studies, Egypt. J. Pet., 26 (2017) 553–563.
[50] Ş. Taşar, A. Özer, A thermodynamic and kinetic evaluation of the adsorption of Pb(II) ions using peanut (*Arachis hypogaea*) shell-based biochar from aqueous media, Pol. J. Environ. Stud., 29 (2020) 293–305.
[51] R. Mudzielwana, M.W. Gitari, P. Ndungu, Performance evaluation of surfactant modified kaolin clay in As(III) and As(V) adsorption from groundwater: adsorption kinetics, isotherms and thermodynamics, Heliyon, 5 (2019) e02756.
[52] M. Đolić, M. Karanac, D. Radovanović, A. Umićević, A. Kapidžić, Z. Veličković, A. Marinković, Ž. Kamberović, Closing the loop: As(V) adsorption onto goethite impregnated coal-combustion fly ash as integral building materials, J. Cleaner Prod., 303 (2021) 126924.
[53] E. Agrafioti, D. Kalderis, E. Diamadopoulos, Arsenic and chromium removal from water using biochars derived from rice husk, organic solid wastes and sewage sludge, J. Environ. Manage., 133 (2014) 309–314.
[54] E. Arco-Lázaro, I. Agudo, R. Clemente, M.P. Bernal, Arsenic(V) adsorption–desorption in agricultural and mine soils: effects of organic matter addition and phosphate competition, Environ. Pollut., 216 (2016) 71–79.
[55] M.S. Rahman, M.W. Clark, L.H. Yee, M.J. Comarmond, T.E. Payne, E.D. Burton, Effects of pH, competing ions and aging on arsenic(V) sorption and isotopic exchange in contaminated soils, Appl. Geochem., 105 (2019) 114–124.
[56] Q. Feng, Z. Zhang, Y. Chen, L. Liu, Z. Zhang, C. Chen, Adsorption and desorption characteristics of arsenic on soils: kinetics, equilibrium, and effect of $Fe(OH)_3$ colloid, H_2SiO_3 colloid and phosphate, Procedia Environ. Sci., 18 (2013) 26–36.
[57] J. Jiang, Z. Dai, R. Sun, Z. Zhao, Y. Dong, Z. Hong, Evaluation of ferrolysis in arsenate adsorption on the paddy soil derived from an oxisol, Chemosphere, 179 (2017) 232–241.
[58] R. Mukhopadhyay, K.M. Manjaiah, S.C. Datta, R.K. Yadav, B. Sarkar, Inorganically modified clay minerals: preparation, characterization, and arsenic adsorption in contaminated water and soil, Appl. Clay Sci., 147 (2017) 1–10.
[59] S. Hafeznezami, A.G. Zimmer-Faust, A. Dunne, T. Tran, C.Yang, J.R. Lam, M.D. Reynolds, J.A. Davis, J.A. Jay, Adsorption and desorption of arsenate on sandy sediments from contaminated and uncontaminated saturated zones: kinetic and equilibrium modeling, Environ. Pollut., 215 (2016) 290–301.
[60] M. Abdelwaheb, K. Jebali, H. Dhaouadi, S. Dridi-Dhaouadi, Adsorption of nitrate, phosphate, nickel and lead on soils: risk of groundwater contamination, Ecotoxicol. Environ. Saf., 179 (2019) 182–187.
[61] Y.S. Ng, B. Sen Gupta, M.A. Hashim, Performance evaluation of natural iron-rich sandy soil as a low-cost adsorbent for removal of lead from water, Desal. Water Treat., 57 (2016) 5013–5024.
[62] A. Augustine, Adsorption–desorption study of heavy metals on sandy-loam soil of sapele metropolis, J. Environ. Sci. Technol. Food Technol., 11 (2017) 17–27.
[63] A. Kushwaha, R. Rani, J.K. Patra, Adsorption kinetics and molecular interactions of lead [Pb(II)] with natural clay and humic acid, Int. J. Environ. Sci. Technol., 17 (2020) 1325–1336.
[64] L. Kalakodio, O.E. Alepu, A. Amenay Zewde, Adsorption and desorption of lead(Pb) in sandy soil treated by various amendments, J. Environ. Anal. Toxicol., 7 (2017).
[65] C. Umeh, J.N. Asegbeloyin, K.G. Akpomie, E.E. Oyeka, A.E. Ochonogor, Adsorption properties of tropical soils from Awka North Anambra Nigeria for lead and cadmium ions from aqueous media, Chem. Afr., 3 (2020) 199–210.
[66] B. Das, N.K. Mondal, R. Bhaumik, P. Roy, Insight into adsorption equilibrium, kinetics and thermodynamics of lead onto alluvial soil, Int. J. Environ. Sci. Technol., 11 (2014) 1101–1114.